Solar Energy Materials & Solar Cells 130 (2014) 27–35

Contents lists available at ScienceDirect

Solar Energy Materials & Solar Cells

journal homepage: www.elsevier.com/locate/solmat

Excimer laser treatment of TiO_2/WO_3 thin films for self-cleaning gasochromic applications: Preparation and characterization

S. Ghayeb Zamharir, M. Ranjbar*, H. Salamati

Department of Physics, Isfahan University of Technology, Isfahan 8415683111, Iran

ARTICLE INFO

Article history:
Received 18 January 2014
Received in revised form
21 May 2014
Accepted 19 June 2014

Keywords:
Tungsten oxide
Titanium oxide
Gasochromic
Pulsed laser deposition
Excimer laser treatment
Photocatalyst

ABSTRACT

Surface poisoning of gasochromic tungsten oxide layers is one of the most challenging effects, which needs to be resolved. In this paper, first amorphous TiO_2/WO_3/glass thin films have been prepared by reactive pulsed laser deposition (PLD) method. Then they were irradiated by a single-pulse of excimer laser (λ=248 nm) with different incident energies (110, 140, 170 and 200 mJ) in order to obtain a thin top layer of anatase TiO_2 (a-TiO_2) with high photocatalytic activity. By means of X-ray diffraction (XRD), it was observed that by excimer laser treatment (ELT) at 110 mJ, a-TiO_2 phase is forming while a mixture of a-TiO_2 and monoclinic WO_3 (m-WO_3) is forming at higher energies. X-ray photoelectron spectroscopy (XPS) revealed that laser treatment removes surface contaminants and hydroxyl groups, increases the W/Ti ratio, shifts surface tungsten oxidation states to lower binding energies and leads to the formation of TiC compound on the surface. The surface morphology of samples was investigated by atomic force microscope (AFM) and field emission scanning electron microscope (FESEM). It was revealed that the surface roughness increases with the laser energy, which is due to an increase in the height of surface granular particles. The films hydrophilicity, measured by water contact angle, was found to increase with the incident laser energy. The photocatalytic activity was investigated by methylene orange (MO) degradation test. It was observed that the sample irradiated at 110 mJ has the most increased photocatalytic activity. The variation of optical transmittance was investigated by UV–vis spectrophotometer. The gasochromic properties of samples with and without laser treatment were compared in the presence of diluted hydrogen (10%H_2/90%Ar) gas.

1. Introduction

Gasochromic WO_3 devices have been gaining importance in recent years due to large number of applications including electrochromic windows [1,2], gasochromic windows [3], displays [4,5] and optical hydrogen sensors [6,7]. WO_3 thin films activated by the noble metal (Pd, Pt, Au) coatings are appropriate candidates in hydrogen sensing industry. The noble metal layer acts as a hydrogen catalyst by which hydrogen molecules are dissociated into H^+-e^- pairs. Double injection of H^+ ions and electrons into WO_3 porous structure changes transparent WO_3 layer to a dark blue state [8,9]. Since the initial step for gasochromic coloring is the dissociation of hydrogen molecules on the catalyst surface, coloring rate depends on the number of catalyst active sites [10]. However, surface poisoning is a well-known issue that threatens the coloring performance of WO_3 thin films [11,12]. This problem arises from the adsorption of gaseous pollutants such as sulfur and carbon monoxide on the surface [13], resulting in the reduction of available sites for hydrogen dissociation and hence a poor gasochromic switching. To solve this problem several researchers have examined various strategies like polydimethylsiloxane (PDMS) protective layer [10], doping catalyst nanoparticles into WO_3 sol matrix via sol–gel route [12] and post-annealing of poisoned thin films [11]. A key limitation of these studies is that they are short-term solutions. In this regard, a more satisfying approach seems to be fabricating a dual functional self-cleaning gasochromic device.

a-TiO_2 is a famous semiconductor with a brilliant antecedent for photocatalytic purposes [14]. It has been found that when a-TiO_2 is irradiated by UV light, active radicals like O_2^- and $OH^\bullet$ are produced on the surface which break down adsorbed contaminations [15]. Therefore, utilizing photocatalytic property of a-TiO_2, a-TiO_2/WO_3 bilayers are likely promising structures to eliminate poisoning of gasochromic devices.

Many methods can be used to deposit a-TiO_2 thin films, involving reactive PLD [16–18], sputtering [19,20] and sol–gel [21], among which PLD is a suitable technique to fabricate stoichiometric metal oxides of high purity under controlled deposition conditions such as oxygen pressure and substrate temperature. To achieve a-TiO_2 thin films via PLD method, a substrate temperature of 400–600 °C is required [22–24]. In TiO_2/WO_3/glass layer systems, this temperature

* Corresponding author. Tel.: +98 31 33913754; fax: +98 31 33912376.
E-mail address: ranjbar@cc.iut.ac.ir (M. Ranjbar).

http://dx.doi.org/10.1016/j.solmat.2014.06.029
0927-0248/

range leads certainly to crystallization of WO_3 layer as well which should be avoided for gasochromic purposes. As reported in our previous study [7], the substrate temperature of 200 °C provides good gasochromic WO_3 thin films. Thus, a surface crystallization technique should be explored to create a-TiO_2 on amorphous WO_3.

Excimer laser treatment (ELT) is an alternative surface modification method which can be applied to obtain thin films with desired structural phases [25]. This method offers a solution to traditional annealing methods [26] because crystal transformations can be obtained within a second at room temperature depending on the pulse duration of laser beam. Previously Overschelde et al. have demonstrated successful anatase crystallization of sputtered TiO_2 thin films by the single-shot of nanosecond KrF eximer laser [26]. In [27] structural modification of WO_3 thin films induced by excimer laser annealing is reported too. To the authors' best knowledge no publication is available in the literature discussing ELT of TiO_2/WO_3 thin films for dual functional self-cleaning gasochromic applications. Therefore, it is of scientific and technological importance to investigate the capability of ELT method for surface crystallization of TiO_2 to have a photocatalytic active surface on the gasochromic layers.

In this paper we first deposited TiO_2/WO_3/glass thin film samples. Then their physical and chemical variations before and after single-shot ELT were investigated by XRD, XPS, AFM, FESEM, water contact angle measurement, MO degradation and UV–vis spectrophotometry techniques. Finally their gasochromic properties were compared. Based on our findings we believe that ELT is an effective tool for dual self-cleaning gasochromic purposes.

2. Experimental

TiO_2/WO_3 thin films were deposited on the ultrasonically cleaned glass substrates by PLD method. First, deposition chamber was evacuated to a pressure of 1×10^{-5} Torr. Then the oxygen (purity 99.99%) pressure was raised to 500 mTorr. 10,000 Total pulses of KrF excimer laser ($\lambda=248$ nm, $f=10$ Hz, $\tau=10$ ns) with 200 mJ energy were delivered to a well pressed high purity WO_3 rotating target at 45° incident angle. The substrate temperature was fixed at 200 °C by means of an electric heater directly placed on the back of substrates. The substrate to WO_3 target distance was 6 cm. Immediately after WO_3 deposition, TiO_2 layer was deposited on the pre-deposited WO_3/glass from a TiO_2 rotating target using 10,000 pulses of KrF laser with 240 mJ energy in the 75 mTorr oxygen pressure. The deposition temperature was kept constant at 200 °C. The distance between TiO_2 target and WO_3/glass substrate was reduced to 4 cm. At the end of deposition process, ELT was applied on the obtained TiO_2/WO_3/glass thin films. The schematic illustration of ELT process is shown in Fig. 1. In ELT process fresh TiO_2/WO_3 bilayer films were exposed normally to the single pulse of KrF laser with approximate 2.5×1 cm^2 spot area in air. The energy of laser pulse was selected to be 110, 140, 170 and 200 mJ which are identical to the laser fluences of about 44, 56, 68 and 80 mJ cm^{-2}. Laser treated TiO_2/WO_3 thin films with above energies are called 110TW, 140TW, 170TW and 200TW samples, respectively.

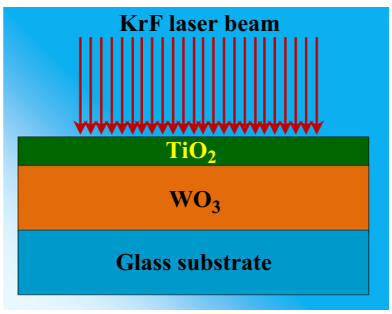

Fig. 1. Schematic representation of ELT process.

To investigate the crystal structure of samples XRD (Philips XPERT MPD) with Cu-Kα source ($\lambda=0.154$ nm) was used. The surface chemical analysis was achieved using XPS with Al anode X-ray source and a hemispherical electron analyzer (Specs model EA10 plus). Binding energies were calibrated against carbon binding energy (284.8 eV). Surface morphology of samples was viewed by AFM (Park Scientific Instruments, AUTOPROBE CP) and FESEM (Hitachi model S4460). The optical transmittance spectra were measured by UV–vis spectrophotometer (PerkinElmer Lambda 25). To study the hydrophilicity property, water contact angle measurement was performed by commercial contact angle meter (Data physics OCA 15 plus). The photocatalytic activity of samples was evaluated by MO degradation test. The samples were placed in a quartz cell containing 4 cm^3 MO (10 ppm) solution. Before testing, they were kept in the dark for 1 h and then irradiated using a UV lamp (Philips TUV 15 W T8, main peak at 254 nm). The intensity of MO absorption peak at 462 nm was measured by UV–vis spectrophotometer at various irradiation time intervals. To observe the gasochromic coloring of various samples they were placed in a sealed chamber containing 10% H_2/Ar gas. To activate the surface of samples against hydrogen, 0.1 cm^3 of 0.2 g/l $PdCl_2$ solution was dropped over the samples.

3. Results and discussion

3.1. X-ray diffraction

In order to explore the effect of laser irradiation on the structural variations in TiO_2/WO_3 bilayer system, XRD patterns were compared for a single-pulse illumination with different incident energies. Fig. 2 represents XRD patterns of as-prepared and those corresponding to laser energies of 110, 140, 170 and 200 mJ per pulse. As can be seen the as-prepared sample is amorphous. However, XRD pattern of 110TW involves a small diffraction peak located around $2\theta=25.4°$ which is due to (101) crystallographic orientation of a-TiO_2 (JCPDS 01-071-1168). When the laser energy increases to 140 mJ (sample 140TW), XRD pattern contains (101) peak of a-TiO_2 with enhanced intensity and some new diffraction peaks. These extra peaks including (200), (210), (021), (211) and (041) planes are related to m-WO_3 (JCPDS 01-075-2072). As can be seen, m-WO_3 (200) peak is more intense than a-TiO_2 (101). Thus, it seems that structural transformation from amorphous to monoclinic is more straightforward for WO_3 sublayer even under illumination by single-pulse. The same issue can be found for the crystallographic variations when the laser energy increases to 170 and 200 mJ; m-WO_3 diffraction peaks become sharper by increase in the amount of laser energy. Meanwhile, (111) plane of m-WO_3 appears. Additionally, m-WO_3 (200) peak becomes stronger than (101) orientation of a-TiO_2.

3.2. X-ray photoelectron spectroscopy

To investigate the surface chemistry variation, elemental and chemical compositions in the process of ELT, XPS was utilized for as-prepared and 200TW typical samples. The corresponding XPS survey scans (0–1200 eV region) are illustrated in Fig. 3(a and b), respectively. The spectra of both samples include major elemental constituents of layers involving Ti, O, and W in addition to the signals of carbon contaminants. The reduction of C_{1s} peak relative intensity after ELT process is due to the carbon removal from the surface; a laser-cleaning effect. Even though TiO_2 layer has been

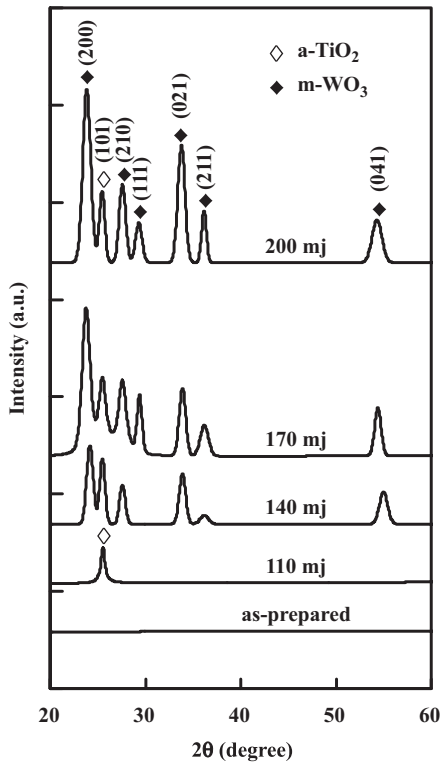

Fig. 2. XRD patterns of TiO_2/WO_3 bilayers before (as-prepared) and after laser irradiation with different energies.

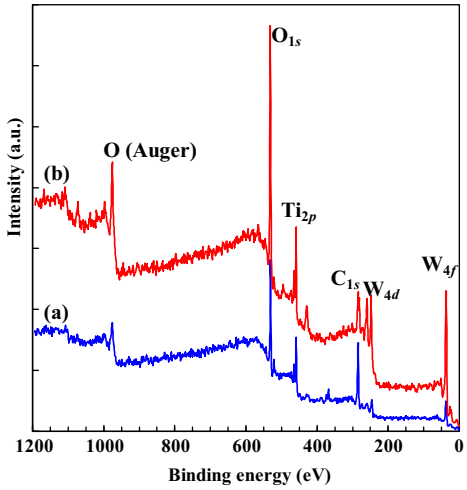

Fig. 3. XPS survey scan of (a) as-prepared and (b) laser irradiated TiO_2/WO_3 thin film with 200 mJ energy (200TW).

deposited on the top of WO_3 layer, some photoelectron signals exist for W_{4f} and W_{4d} over the spectrum of as-prepared sample. These signals are likely from the inhomogeneous growth of TiO_2 layer, presence of thick buried droplets of WO_3 and/or even surface cracks. Two later ones are common effects during plume propagation and deposition in PLD process [28].

To study the surface compositions in more details, high resolution XPS spectra of O_{1s}, C_{1s}, Ti_{2p} and W_{4f} core levels were deconvoluted into some constructing peaks (Fig. 4(a–d)). O_{1s} core level spectra of as-prepared and 200TW samples are presented in Fig. 4(a). For the as-prepared sample, O_{1s} peak is asymmetric consisting of two deconvoluted components at 530.4 eV assigned to the oxygen in bonding with Ti and W, and at 531.8 eV binding energy which is associated to the hydroxyl groups and/or C=O bonds [29]. After the laser treatment, the O_{1s} spectrum is rather symmetric involving a main peak located at 530.7 eV and a very weak peak at 531.7 eV. Same as previous case, the former peak can be related to structural oxygen and the later one to the hydroxyl groups. Comparing with the as-prepared sample the hydroxyl counterpart is extremely low. Therefore, the hydroxyl group removal during laser–surface interaction is also an issue like to carbon cleaning. Thus, XPS data of carbon and oxygen proposes that surface contaminations and hydroxyl groups have been erased from the surface composition.

Fig. 4(b) shows the high resolution core-level spectra of C_{1s} before and after ELT process. Before the laser treatment, only one peak at 284.8 eV exists which is assigned to C–C bond. In addition to this peak, one extra peak appears at 281.4 eV after laser irradiation, which is attributed to TiC composition [31]. It seems that as a result of the ELT process new surface chemical compounds could be created in our samples.

In Fig. 4(c) for as-prepared sample the deconvolution of Ti_{2p} peak gives two $Ti_{2p3/2}$ and $Ti_{2p1/2}$ lines located at 458.7 and 464.4 eV, respectively. Additionally, the difference between Ti_{2p} doublet lines is 5.7 eV which is consistent with level splitting theory corresponding to the Ti^{4+} oxidation state [31]. Based on XPS, it can be found that ELT does not shift Ti_{2p} doublet considerably. Thus, the surface chemical composition of TiO_2 is not affected by laser treatment. However, it will be shown that this is not the case for tungsten binding energy.

Since Ti_{3p} binding energy exists in W_{4f} region [30,32], to study TiO_2/WO_3 bilayers Ti_{3p} line was also considered. In general, W_{4f} involves doublet with different peak areas; the peak at lower binding energy ($W_{4f7/2}$) has higher intensity up to 4/3 times of the peak at higher energy ($W_{4f5/2}$). However, in our case the peak area order is quite opposite indicating that within W_{4f} region near to $W_{4f5/2}$, Ti_{3p} peak must be taken into account. In the spectrum of as-prepared sample $W_{4f7/2}$ and $W_{4f5/2}$ components are positioned at 35.2 and 37.5 eV (Fig. 4(d)), characteristics of W^{6+} state [33]. The separation energy of $W_{4f7/2}$ and $W_{4f5/2}$ components is about 2.3 eV which is in good agreement with other reports [34]. Moreover, for sample 200TW $W_{4f7/2}$ and $W_{4f5/2}$ binding energies shift toward lower values of 33.7 and 35.6 eV, respectively. One possible implication for this shift may be the laser-induced reduction of tungsten oxidation states. According to [35] the binding energies of W_{4f} doublet related to W^{4+} states are 33.6 and 35.75 eV. In [36] 33.7 and 35.8 eV are reported for W_{4f} lines corresponding to the W^{4+} oxidation state. Therefore, W^{6+} to W^{4+} conversion is more feasible than any change in Ti oxidation states in laser treated TiO_2/WO_3 bilayers.

Table 1 summarizes the surface concentration percentages of W, Ti, O and C as well as W/Ti elemental ratio for as-prepared and 200TW samples. From the table, W/Ti molar ratio increases from 2.7 to 8.1 (up to 3 times) after laser irradiation. Seemingly laser treatment could increase the surface contribution of WO_3 beneath layer for example via surface melting and mixing with TiO_2 layer. Moreover, the oxygen surface concentration drops from 34.0% to 30.1%. Some part of this oxygen change may be related to bond dissociation in W–O and formation of reduced states such as W^{4+} which is confirmed by XPS spectra of W_{4f} (Fig. 4(d)).

3.3. Morphology

The effect of laser energy in the ELT process on TiO_2/WO_3 surface morphology was studied by means of AFM and FESEM. Fig. 5 shows 2D AFM images of as-prepared and laser treated samples as well as some selected line profiles. For more clarity the RMS surface roughness and the surface ratio values are presented in Table 2. From AFM image of as-prepared sample, the surface contains granular particles. This is likely due to an island-growth mode throughout deposition of TiO_2 at substrate temperature of 200 °C. The surface of sample 110TW consists of nearly spherical

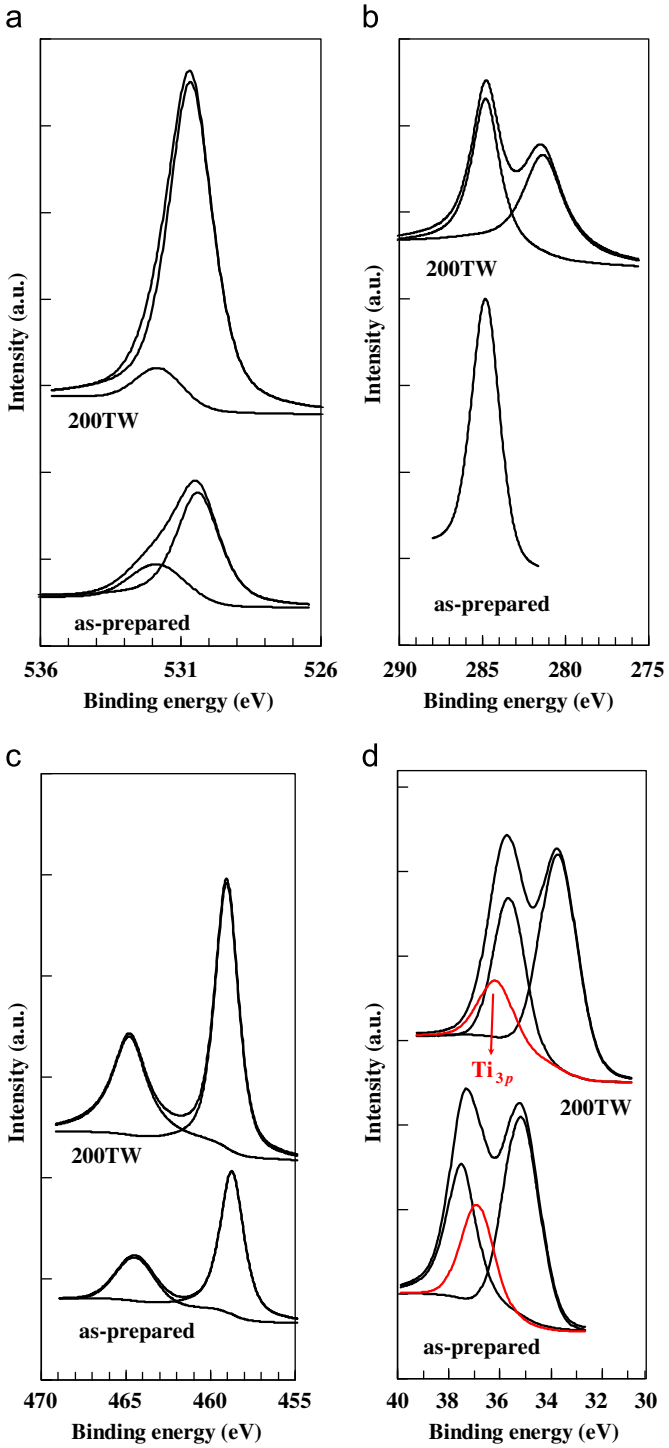

Fig. 4. High resolution core level spectra of (a) O_{1s}, (b) C_{1s}, (c) Ti_{2p}, and (e) W_{4f} for as-prepared and 200TW samples.

particles which are forming an almost uniform surface. Increasing laser energy to 140 mJ (sample 140TW) leads to the surface roughening and formation of larger particles. This effect possibly originates from the process of surface melting followed by re-solidification [37]. By increasing the laser energy to 170 and 200 mJ, one can see that the particles are widened and the surface roughening progresses more rapidly. From Table 2 it can be seen that surface roughness increases with laser energy. The surface roughness of the as-prepared sample is 16.3 nm while it reaches 57.3 nm for the laser treated film at 200 mJ. The surface ratio, which is defined as the ratio of the actual surface including total surface area of rough film to the area of AFM image window, increases slightly with laser energy. The higher the surface ratio, the higher the gas-surface reaction rate constant, which may be an important effect in diffusion controlled gasochromic regime. From line profiles of AFM images one can estimate the height alteration across the surface which is described as the difference between maximum and minimum heights (ΔZ). The values of ΔZ are 64, 74, 125, 240 and 296 nm for as-prepared, 110TW, 140TW, 170TW and 200TW samples, respectively. Therefore, laser treatment at higher laser energies creates a rougher surface. Meanwhile, in line profile of all samples there exists multiple peaks corresponding to the

Table 1
Elemental concentration percentages of W, Ti, O and C and W/Ti elemental ratio for as-prepared and 200TW samples.

Sample	Elemental concentration (%)				W/Ti
	W	Ti	O	C	Molar ratio
As-prepared	18.7	7	34	40.2	2.7
200TW	43	5.3	30	21.6	8.1

position of each grain along the cross lines. These peaks show higher height of grains relative to the neighboring points.

To detail the laser-induced variations of surface morphology, the FESEM images of as-prepared and a typical laser-treated film (200TW) are presented in Fig. 6(a and b). From the inset of Fig. 6(a), one can see that the as-prepared sample has cauliflower-like grains together with many spherical-shaped micro-particles. As it was mentioned previously the presence of this kind of spherical particles, known as droplets, is common in pulsed laser deposition and they are ejected from the target surface when it is irradiated by a focused pulsed laser beam. Moreover, as seen in Fig. 6(a) the cauliflower-like islands are separated by many observable cracks which are developed as the films gets thicker during deposition and undergoes non-uniform surface tensions. These types of fractured surface are usually seen among columnar growth of metal oxide films using physical vapor deposition (PVD) methods, e.g. PLD and provide porous structures. However, the surface of 200TW sample consists of a heterogeneous morphology; some dense island-like regions (denoted D) and a granular background consisting of nanoparticles with a small average size less than 100 nm (denoted by G). The dense island-like species resemble molten zones which have been cooled after a process of melting and then became re-solidified. Regarding to line profile data obtained from AFM images in previous part, the height of dense island-like regions is of the order of 100 nm. To explain the FESEM results, one can state that laser beam initially melts the upper TiO_2 layer, and then the molten species diffuse across the surface and coagulate to form the dense island-like particles. So probably these kinds of particles are Ti-rich.

3.4. Optical properties

To determine the influence of laser energy on optical properties of TiO_2/WO_3 thin films, UV–vis transmittance spectra of as-prepared and laser treated samples were recorded. Optical transmittance spectra within 300–1100 nm wavelength region are shown in Fig. 7 (a–e) for different samples. It can be seen that the as-prepared sample has the highest optical transmittance with an average value of 90.3% among other laser treated samples. However, in the cases of processed samples (110TW–200TW) depending on the laser energy transmittance gradually decreases. The average value of transmittance at 110 mJ energy is 70.8% while it gets 26.2% for laser irradiated sample at 200 mJ energy. It should be mentioned that after laser exposure, the color of transparent TiO_2/WO_3 thin films turned into a light gray-blue state. With regard to XPS findings, this color change could be associated to surface reduction of WO_3 and partial formation of W^{4+} beside W^{6+} states, responsible for the formation of color centers [38], while no trace of lower oxidation number has been detected for Ti ions. Therefore, we can conclude that the reduction of W^{6+} cations is responsible for color change in our research rather than Ti^{4+}. Meanwhile, surface roughness is an important issue affecting the optical properties of thin films. A rough surface scatters most of the incident light, resulting in decrease of films optical transmittance [39]. Furthermore, the optical spectrum of each 170TW and 200TW samples has a broad peak around 350–500 nm which is associated to the light blue color mentioned above.

The optical band gaps of samples were deduced from the extrapolation of optical absorption spectra using Tauch equation [40]. The optical band gap was found to be 3.18, 3.16, 3, 2.94 and 2.94 eV for as-prepared, 110TW, 140TW, 170TW and 200TW samples, respectively. Generally, by increasing laser energy the band gap value decreases which is probably due to the formation of oxygen vacancy [40] and low oxidation states of tungsten ions as mentioned in XPS section. According to XPS analysis and changes in optical transmittance spectra one can say that to avoid formation of excess oxygen vacancies as a source of optical deterioration, ELT should be done below a certain threshold energy.

3.5. Hydrophilicity properties

In laser treatment process, the effect of laser energy on hydrophilicity properties of TiO_2/WO_3 bilayers was explored using water contact angle measurement. The water contact angle vs. laser incident energy is given in Fig. 8. The inset of the figure shows photographs of water droplets placed on the surface of different samples. One can see that the contact angle decreases from about 80° to 72° when the TiO_2/WO_3 bilayer is irradiated by a 110 mJ laser pulse. At 140 mJ the contact angle drops noticeably to about 47° and then by further increase of energy to 170 and 200 mJ, reduces to about 42° and 33°, respectively. So, depending on the laser energy TiO_2/WO_3 surface becomes more hydrophilic. Surface hydrophilicity modification of KrF laser treated TiO_2 thin films was reported by Bayati et al. too [29]. They proposed that laser-induced oxygen deficiencies are filled by dissociative adsorption of water molecules, hence the water contact angle begins to diminish and hydrophilicity increases.

Additionally, it is well-known that hydrophilicity properties of a layer can be related to surface microstructure by the Wenzel model [41] which is described as follows:

$$\cos\theta = r\cos\alpha \quad (1)$$

where θ is the contact angle of a liquid on a rough surface, α is the contact angle of a liquid on a smooth surface (Young's angle) and r is the surface area ratio as calculated in Table 2. According to the Wenzel model surface roughness can intensify wetting feature of a layer. To understand whether surface roughness is a major factor in hydrophilicity property of our samples or not, Young's contact angle (α) of different samples was calculated using Eq. (1). The results are shown in Fig. 8. The differences between α and θ angles especially in the case of 140TW, 170TW and 200TW samples show that in addition to oxygen vacancies resulted from XPS, the surface roughness has an important role on surface hydrophilicity in our samples.

3.6. Photocatalytic activity

In order to examine the photocatalytic activity of as-prepared and laser treated samples, MO degradation test was performed as described in experimental section. MO decomposition percentage of different samples vs. UV irradiation time is illustrated in Fig. 9(a) at early preparation stages. The as-prepared sample (TW), which is amorphous in nature has a rather low photocatalytic activity. Although the majority of good photocatalytic titanium oxide products reported so far are usually a-TiO_2, reports on negligible photocatalytic activity exist for amorphous films too [42]. From Fig. 9(a) the photocatalytic activity has been affected by laser treatment. Slight enhancements can be observed for 140TW, 170TW and 200TW samples which are almost of the same order. However, there is a significant increase in MO degradation rate for 110TW sample. This distinguished photocatalytic behavior of 110TW might be addressed by XRD results which has confirmed the crystal structure of a-TiO_2/WO_3. Given these explanations, it would be concluded that

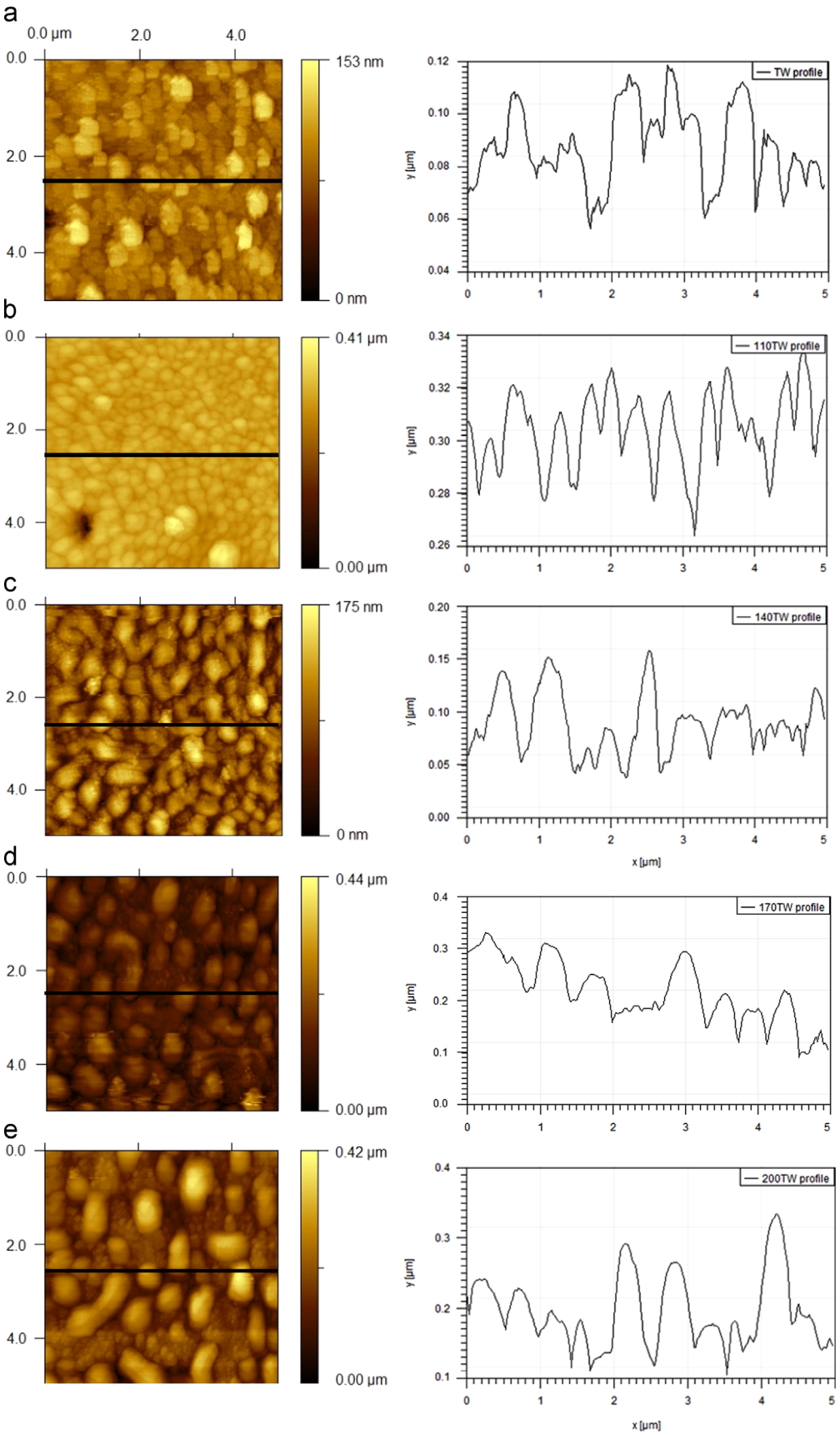

Fig. 5. AFM images and corresponding line profiles of different samples (a) as-prepared, (b) 110TW, (c) 140TW, (d) 170TW and (e) 200TW.

Table 2
RMS surface roughness and the surface ratio for different samples.

Sample	As-prepared	110TW	140TW	170TW	200TW
RMS (nm)	16.3	23.4	26.4	44.2	57.3
Surface ratio	1.04	1.06	1.11	1.21	1.19

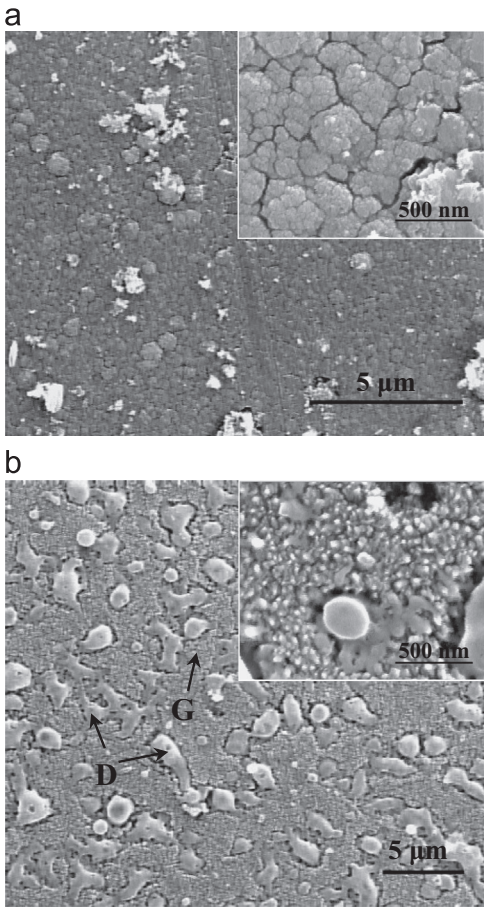

Fig. 6. FESEM images of (a) as-prepared and (b) 200TW samples.

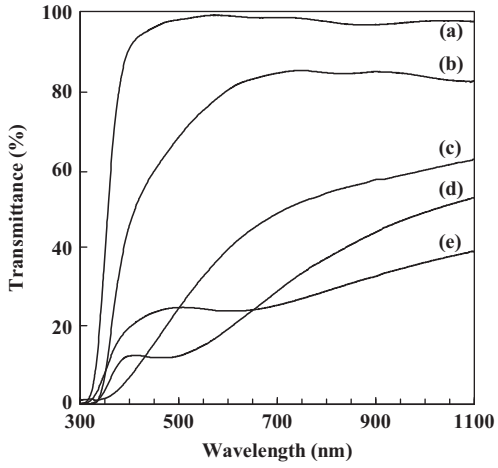

Fig. 7. Optical transmittance spectra of (a) as-prepared, (b) 110TW, (c) 140TW, (d) 170TW, and (e) 200TW samples.

crystallization of WO_3 layer in samples 140TW–200TW prevents improvement of photocatalytic performance. In contrast, a-TiO_2 is the dominant crystal phase of sample 110TW. Smith et al. have observed

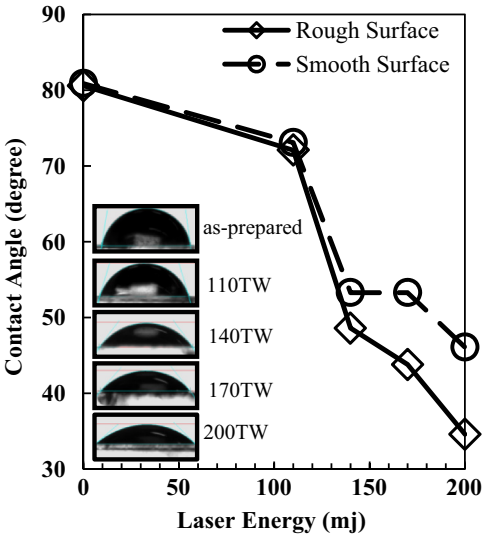

Fig. 8. Water contact angle on rough and smooth surface vs. laser energy. (inset) photographs of water droplet on the as-prepared and laser treated films.

the reduction of photocatalytic activity of TiO_2/WO_3 bilayers when WO_3 transformed from amorphous to orthorhombic (o-WO_3) by post-annealing at 400 °C. They proposed that electron–hole separation decreases for TiO_2/o-WO_3 due to the fact that the conduction and valance bands of o-WO_3 are far from those of TiO_2 [43]. Besides, from XPS it was found that the reduction of tungsten oxidation states, desorption of hydroxyl groups and formation of extra oxygen vacancies occur during laser treatment. It is expected that surface chemical variations do not progress notably across the films under low laser energy irradiation. Hence, in the case of 110 mJ energy, the low energy of incident beam may be responsible for the unique photocatalytic behavior at a certain energy value.

In order to examine the stability of photocatalytic activity of TiO_2/WO_3 samples, the photocatalytic tests were repeated after six months. The results (Fig. 9(b)) propose that there is an almost good stability against aging. Although sample 110TW has the highest photocatalytic activity among the other samples yet, there is a drop in its activity after six months comparing with its virgin type. The origin of this drop is not very clear but it may be due to the absorption of some poisoning species deep into the layer from laboratory environment. Therefore, aging has no sufficient impact on photocatalytic activity of laser treated TiO_2/WO_3 samples.

3.7. Gasochromic test

To investigate the gasochromic response of as-prepared and laser treated TiO_2/WO_3 thin films, samples were placed in a sealed hydrogen-containing chamber. Before the hydrogen flows, the surface of samples was activated by wet $PdCl_2$ drop similar to our previous work [7]. Fig. 10(top) represents samples photographs of different coloring steps with 60 min total time after hydrogen exposure. From the figure, it can be seen that coloring starts from edges. This phenomenon is consistent with our previous study in which coloring of $PdCl_2$(aq)/WO_3 thin films have started from substrate–liquid–gas triple points. From Fig. 10 one can see that samples TW (as-prepared) and 110TW get almost the full colored state after 60 min hydrogen exposure. Moreover, the coloring of the sample 110TW is faster than that of TW. To compare the optical properties of colored samples in more detail, optical density functions (defined as $\Delta OD = -\ln [T_c/T_b]$; T_c and T_b are transmittance at colored and bleached states, respectively) are plotted in Fig. 10 (bottom). As can be seen the ΔOD of

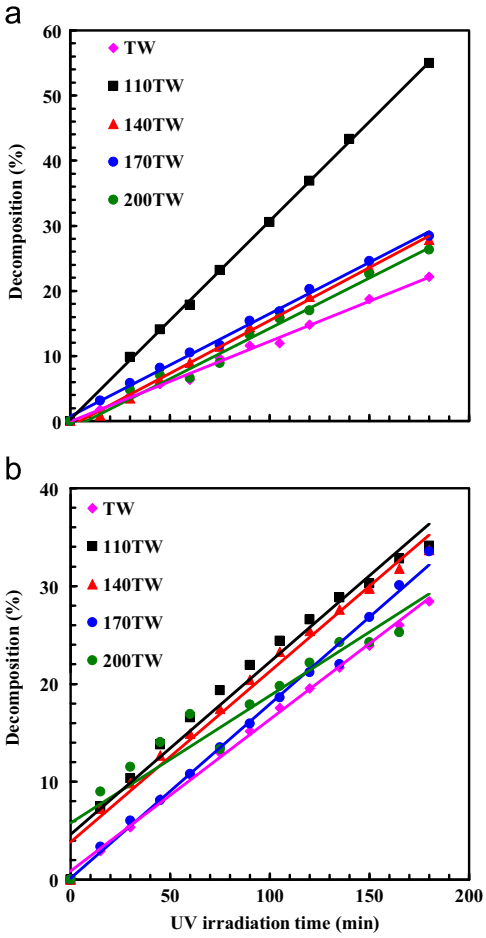

Fig. 9. MO degradation percentage for TiO_2/WO_3 samples with and without ELT process at different laser energies, (a) after deposition process and (b) after six months aging.

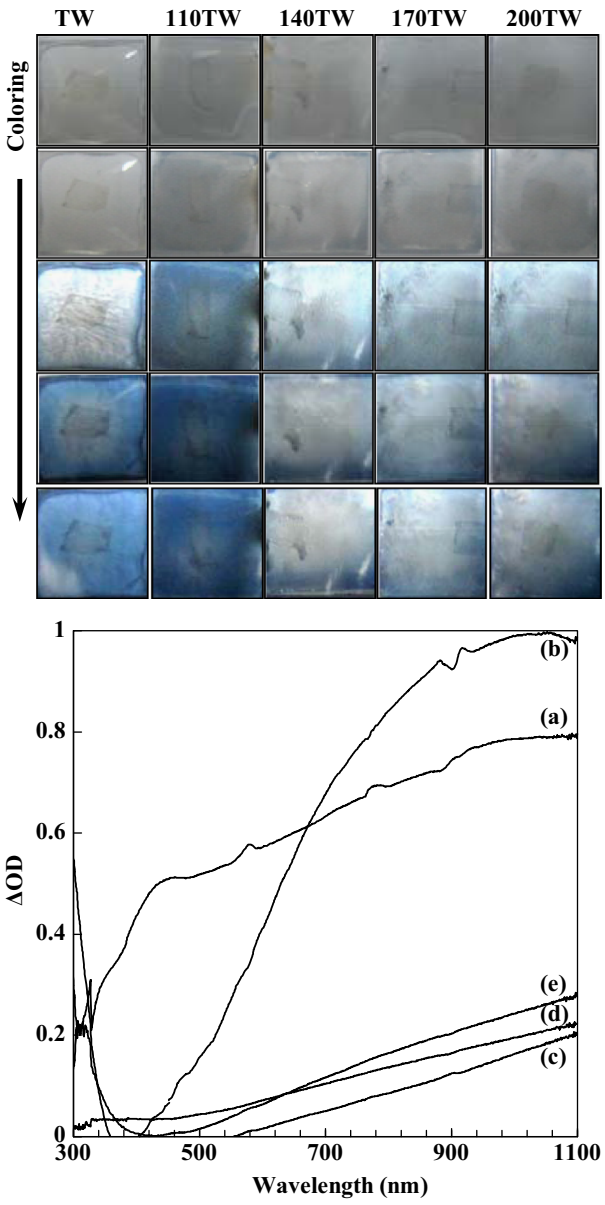

Fig. 10. (Top) Photographs of different samples during gasochromic coloration at different stages. (Bottom) Optical density functions of (a) as-prepared, (b) 110TW, (c) 140TW, (d) 170TW and (e) 200TW colored samples. (For interpretation of the references to color in this figure legend, the reader is referred to the web version of this article.)

sample 110TW is considerably high in the visible to NIR region among the other samples. For all cases, ΔOD is higher at NIR region compared with the visible region as it is well-known for the IR absorption property of bronze tungsten oxide films. The poor coloring effect of the samples 140TW–200TW can be attributed to their crystalline nature arising from the ELT process. Although the WO_3 layer of the sample TW is amorphous in nature, the presence of the continuous layer of TiO_2 decreases the interlayer diffusion of hydrogen gas. Only for the sample 110TW there is an amorphous WO_3 layer with island-like TiO_2 top-layer (see the FESEM images). To sum up briefly it seems that the laser treatment of TiO_2/WO_3 at 110 mJ energy is the optimum condition under which good photocatalytic and gasochromic activity could be obtained.

4. Conclusion

This paper aims to present dual functional self-cleaning gasochromic TiO_2/WO_3 thin films as a novel solution for poisoning of gasochromic devices. Excimer laser treatment (ELT) as a surface modification tool was used to make the surface of pre-amorphous TiO_2/WO_3 partially crystallized to a-TiO_2. In our experimental conditions, 110 mJ laser energy provides the best photocatalytic activity. It has been demonstrated that increasing laser energy leads to the formation of an a-TiO_2/m-WO_3 mixture as well as a more hydrophilic surface with enhanced roughness. Furthermore, laser treatment increases W/Ti ratio on the surface of our samples which is probably due to surface melting followed by re-solidification. The as-prepared and 110TW samples showed good gasochromic coloring. Therefore, laser treated TiO_2/WO_3 bilayers at 110 mJ energy can be used for both gasochromic and self-cleaning applications. However, further investigations will be needed to find the optimum conditions of laser treatment in order to have durable thin films with a fast coloring response.

Acknowledgments

The authors would like to thank the Iranian National Science Foundation (INSF) for their financial support (Grant no. 89001655). Also Mr. Modabber-Asl is acknowledged for his kind help in the PLD Lab.

References

[1] C.G. Granqvist, Handbook of Inorganic Electrochromic Materials, Elsevier Science, 1995.
[2] S.K. Deb, Opportunities and challenges in science and technology of WO_3 for electrochromic and related applications, Sol. Energy Mater. Sol. Cells 92 (2008) 245–258.
[3] V. Wittwer, M. Datz, J. Ell, A. Georg, W. Graf, G. Walze, Gasochromic windows, Sol. Energy Mater. Sol. Cells 84 (2004) 305–314.
[4] X. Cui, H. Zhang, X. Dong, H. Chen, L. Zhang, L. Guo, J. Shi, Electrochemical catalytic activity for the hydrogen oxidation of mesoporous WO_3 and WO_3/C composites, J. Mater. Chem. 18 (2008) 3575–3580.
[5] M. Deepa, T. Saxena, D. Singh, K. Sood, S. Agnihotry, Spin coated versus dip coated electrochromic tungsten oxide films: structure, morphology, optical and electrochemical properties, Electrochim. Acta 51 (2006) 1974–1989.
[6] C.-C. Chan, W.-C. Hsu, C.-C. Chang, C.-S. Hsu, Hydrogen incorporation in gasochromic coloration of sol–gel WO_3 thin films, Sens. Actuators B: Chem. 157 (2011) 504–509.
[7] M.A. Behbahani, M. Ranjbar, P. Kameli, H. Salamati, Hydrogen sensing by wet-gasochromic coloring of $PdCl_{2(aq)}/WO_3$ and the role of hydrophilicity of tungsten oxide films, Sens. Actuators B: Chem. 188 (2013) 127–136.
[8] J.G. Zhang, D.K. Benson, C.E. Tracy, S.K. Deb, A. Czanderna, C. Bechinger, Chromic mechanism in amorphous WO_3 films, J. Electrochem. Soc. 144 (1997) 2022–2026.
[9] S.-H. Lee, M.J. Seong, H.M. Cheong, E. Ozkan, E.C. Tracy, S.K. Deb, Effect of crystallinity on electrochromic mechanism of Li_xWO_3 thin films, Solid State Ion. 156 (2003) 447–452.
[10] R. Ghosh, M.B. Baker, R. Lopez, Optical properties and aging of gasochromic WO_3, Thin Solid Films 518 (2010) 2247–2249.
[11] J.Y. Luo, L. Gong, H.D. Tan, S.Z. Deng, N.S. Xu, Q.G. Zeng, Y. Wang, Study of the catalyst poisoning and reactivation of Pt nanoparticles on the surface of WO_3 nanowire in gasochromic coloration, Sens. Actuators B: Chem. (2012).
[12] D. Li, G. Wu, G. Gao, J. Shen, F. Huang, Ultrafast coloring-bleaching performance of nanoporous WO_3–SiO_2 gasochromic films doped with Pd catalyst, ACS Appl. Mater. Interfaces 3 (2011) 4573–4579.
[13] A. Georg, W. Graf, R. Neumann, V. Wittwer, Stability of gasochromic WO_3 films, Sol. Energy Mater. Sol. Cells 63 (2000) 165–176.
[14] K. Nakata, A. Fujishima, TiO_2 photocatalysis: design and applications, J. Photochem. Photobiol. C: Photochem. Rev. 13 (2012) 169–189.
[15] W. Thongsuwan, T. Kumpika, P. Singjai, Effect of high roughness on a long aging time of superhydrophilic TiO_2 nanoparticle thin films, Curr. Appl. Phys. 11 (2011) 1237–1242.
[16] M. Walczak, E. Papadopoulou, M. Sanz, A. Manousaki, J. Marco, M. Castillejo, Structural and morphological characterization of TiO_2 nanostructured films grown by nanosecond pulsed laser deposition, Appl. Surf. Sci. 255 (2009) 5267–5270.
[17] C. Sima, C. Grigoriu, C. Viespe, I. Pasuk, E. Matei, Titanium oxide thin films produced by pulsed laser deposition, J. Optoelectron. Adv. Mater. 11 (2009) 826–830.
[18] Y. Xu, M. Shen, Fabrication of anatase-type TiO_2 films by reactive pulsed laser deposition for photocatalyst application, J. Mater. Process. Technol. 202 (2008) 301–306.
[19] P. Kondaiah, M.C. Sekhar, S.J. Chandra, R. Martins, S. Uthanna, E. Elangovan, Influence of substrate bias voltage on the physical, electrical and dielectric properties of RF magnetron sputtered TiO_2 films, IOP Conference Series: Materials Science and Engineering, IOP Publishing, Madrid, Spain (2012) 012005.
[20] M. Kitano, K. Iyatani, E. Afsin, Y. Horiuchi, M. Takeuchi, S.-H. Cho, M. Matsuoka, M. Anpo, Photocatalytic oxidation of 2-propanol under visible light irradiation on TiO_2 thin films prepared by an RF magnetron sputtering deposition method, Res. Chem. Intermed. 38 (2012) 1249–1259.
[21] K. Zheng, W. Liang, J.J. Wang, C. Rüssel, Preparation and characterization of TiO_2 photocatalytic thin film prepared by sol–gel dip coating, Adv. Mater. Res. 476 (2012) 2398–2402.
[22] Y. Xu, M. Shen, Anatase TiO_2 films fabricated by pulsed laser deposition using Ti target, Appl. Phys. A 94 (2009) 275–280.
[23] X.-S. Zhou, Y.-H. Lin, B. Li, L.-J. Li, J.-P. Zhou, C.-W. Nan, Processing and characterization of TiO_2 film prepared on glass via pulsed laser deposition, J. Phys. D: Appl. Phys. 39 (2006) 558.
[24] Y. Choi, S. Yamamoto, T. Umebayashi, M. Yoshikawa, Fabrication and characterization of anatase TiO_2 thin film on glass substrate grown by pulsed laser deposition, Solid State Ion. 172 (2004) 105–108.
[25] O. Van Overschelde, T. Delsate, R. Snyders, Determination of the melting threshold of TiO_2 thin films processed by excimer laser irradiation, J. Appl. Phys. 111 (2012) 123108-1–123108-4.
[26] O.V. Overschelde, G. Guisbiers, M. Wautelet, Nanocrystallization of anatase or rutile TiO_2 by laser treatment, J. Phys. Chem. C 113 (2009) 15343–15345.
[27] T. Nakajima, T. Kitamura, T. Tsuchiya, Visible light photocatalytic activity enhancement for water purification in Cu (II)-grafted WO_3 thin films grown by photoreaction of nanoparticles, Appl. Catal. B: Environ. 108 (2011) 47–53.
[28] M. Ohring, Materials Science of Thin Films, second ed., Academic press, San Diego, 2002.
[29] M. Bayati, S. Joshi, R. Molaei, R. Narayan, J. Narayan, Ultrafast switching in wetting properties of TiO_2/YSZ/Si(001) epitaxial heterostructures induced by laser irradiation, J. Appl. Phys. 113 (2013) 063706-1–063706-7.
[30] S. Komornicki, M. Radecka, P. Sobaś, Structural properties of TiO_2–WO_3 thin films prepared by rf sputtering, J. Mater. Sci.: Mater. Electron. 15 (2004) 527–531.
[31] L. Mai, D. Wang, S. Zhang, Y. Xie, C. Huang, Z. Zhang, Synthesis and bactericidal ability of Ag/TiO_2 composite films deposited on titanium plate, Appl. Surf. Sci. 257 (2010) 974–978.
[32] J.H. Pan, W.I. Lee, Preparation of highly ordered cubic mesoporous WO_3/TiO_2 films and their photocatalytic properties, Chem. Mater. 18 (2006) 847–853.
[33] H. Bai, N. Su, W. Li, X. Zhang, Y. Yan, P. Li, S. Ouyang, J. Ye, G. Xi, $W_{18}O_{49}$ nanowire networks for catalyzed dehydration of isopropyl alcohol to propylene under visible light, J. Mater. Chem. A (2013) 6125–6129.
[34] S.A.K. Leghari, S. Sajjad, J. Zhang, Large mesoporous micro-spheres of WO_3/TiO_2 composite with enhanced visible light photo activity, RSC Advances 3 (2013) 15354–15361.
[35] G. Leftheriotis, S. Papaefthimiou, P. Yianoulis, A. Siokou, Effect of the tungsten oxidation states in the thermal coloration and bleaching of amorphous WO_3 films, Thin Solid Films 384 (2001) 298–306.
[36] C. Guo, S. Yin, Q. Dong, T. Sato, The near infrared absorption properties of $W_{18}O_{49}$, R. Soc. Chem. Adv. 2 (2012) 5041–5043.
[37] M.-Y. Pu, J.-Z. Chen, I. Cheng, KrF excimer laser irradiated nanoporous TiO_2 layers for dye-sensitized solar cells: influence of laser power density, Ceram. Int. (2013).
[38] S.-H. Lee, H.M. Cheong, J.-G. Zhang, A. Mascarenhas, D.K. Benson, S.K. Deb, Electrochromic mechanism in a-WO_{3-y} thin films, Appl. Phys. Lett. 74 (1999) 242–244.
[39] K. Lethy, D. Beena, R. Vinod Kumar, V. Mahadevan Pillai, V. Ganesan, V. Sathe, Structural, optical and morphological studies on laser ablated nanostructured WO_3 thin films, Appl. Surf. Sci. 254 (2008) 2369–2376.
[40] K. Lethy, D. Beena, R.V. Kumar, V.M. Pillai, V. Ganesan, V. Sathe, D. Phase, Nanostructured tungsten oxide thin films by the reactive pulsed laser deposition technique, Appl. Phys. A 91 (2008) 637–649.
[41] M. Mirshekari, R. Azimirad, A. Moshfegh, Superhydrophilic stability enhancement of RF co-sputtered $Ti_xSi_{1-x}O_2$ thin films in dark, Appl. Surf. Sci. 256 (2010) 2500–2506.
[42] J.C. Yu, L. Zhang, Z. Zheng, J. Zhao, Synthesis and characterization of phosphated mesoporous titanium dioxide with high photocatalytic activity, Chem. Mater. 15 (2003) 2280–2286.
[43] W. Smith, Y. Zhao, Enhanced photocatalytic activity by aligned WO_3/TiO_2 two-layer nanorod arrays, J. Phys. Chem. C 112 (2008) 19635–19641.